RSC Advances

PAPER

View Article Online
View Journal | View Issue

Cite this: *RSC Adv.*, 2024, **14**, 33524

Electric field enhances the electronic and diffusion properties of penta-graphene nanoribbon anodes in lithium-ion batteries†

Thi Nhan Tran, [a] Nguyen Vo Anh Duy,[b] Nguyen Hoang Hieu, [c] Truc Anh Nguyen,[d] Nguyen To Van,[e] Thi Viet Bac Phung,[f] Yohandys A. Zulueta, [g] Minh Tho Nguyen, [hi] Peter Schall[j] and Minh Triet Dang *[c]

Enhancement of the ionic conductivity and reduction of diffusion barriers of lithium-ion batteries are crucial for improving the performance of the fast-growing energy storage devices. Recently, the fast-charging capability of commercial-like lithium-ion anodes with the smallest modification of the current manufacturing technology has been of great interest. We used first principles methods computations with density functional theory and the climbing image-nudged elastic band method to evaluate the impact of an external electric field on the stability, electronic band gap, ionic conductivity, and lithium-ion diffusion coefficient of penta-graphene nanoribbons upon lithium adsorption. By adsorbing a lithium atom, these semiconductor nanoribbons become metal with a formation energy of −0.22 eV, and an applied electric field perpendicular to the surface of these nanoribbons further stabilizes the structure of these lithium-ion systems. Using the Nernst–Einstein relation, in the absence of an electric field, the ionic conductivity of these penta-graphene nanoribbons amounts to 1.24×10^{-4} S cm^{-1}. In the presence of an electric field, this conductivity can reach a maximum value of 8.89×10^{-2} S cm^{-1}, emphasizing the promising role of an electric field for supporting fast-charging capability. Our results highlight the role of an external electric field as a novel switch to improve the efficiency of lithium-ion batteries with penta-graphene nanoribbon electrodes and open a new horizon for the use of pentagonal materials as anode materials in the lithium-ion battery industry.

Received 28th July 2024
Accepted 15th October 2024

DOI: 10.1039/d4ra05464d

rsc.li/rsc-advances

1. Introduction

The lithium-ion rechargeable battery is a fast-growing industry for mobile devices and electric vehicles.[1] Due to the enormous demand fromsociety and the shortage of raw materials supply, the cost of rechargeable lithium-ion batteries (LIBs) is currently high and keeps increasing.[2] This drawback limits the applicability of these types of batteries both in industries and for societal needs. The urgent need is thus to reduce the cost for fabricating LIBs and improve the electrochemical performance such as high reversible capacity, high conductivity, reasonable cycling life and environmentally friendly manufacturing. To boost commercial mobile devices and electric vehicles, besides an increase of the storage capacity of the batteries, a fast-charging capability is urgently needed. For this purpose, reduction of the energy barrier for lithium-ion diffusion is of crucial importance to improve the electrochemical performance of LIBs.

Typical LIBs consist of both anode and cathode electrodes, a separator, and all immersed electrolyte solution. To fulfil the aforementioned requirements, the critical task is to improve the performance of cathode and/or anode electrode materials. Several commercial types of cathode electrode materials for

[a]*Faculty of Fundamental Sciences, Hanoi University of Industry, 298 Cau Dien, Bac Tu Liem, Hanoi, Vietnam*
[b]*FPT University, 600 Nguyen Van Cu, Ninh Kieu, Can Tho, Vietnam*
[c]*Department of Physics Education, Can Tho University, 3/2 Street, Ninh Kieu, Can Tho, Vietnam. E-mail: dmtriet@ctu.edu.vn*
[d]*Faculty of Mechanics, Can Tho University of Technology, 256 Nguyen Van Cu Street, Ninh Kieu, Can Tho, Vietnam*
[e]*Faculty of Chemico-Physical Engineering, Le Quy Don Technical University, Ha Noi, Vietnam*
[f]*Center for Environmental Intelligence and College of Engineering & Computer Science, VinUniversity, Hanoi, Vietnam*
[g]*Departamento de Física, Facultad de Ciencias Naturales y Exactas, Universidad de Oriente, Santiago de Cuba, CP 90500, Cuba*
[h]*Laboratory for Chemical Computation and Modeling, Institute for Computational Science and Artificial Intelligence, Van Lang University, Ho Chi Minh City, Vietnam*
[i]*Faculty of Applied Technology, School of Technology, Van Lang University, Ho Chi Minh City, Vietnam*
[j]*Van der Waals-Zeeman Institute, University of Amsterdam, Science Park 904, Amsterdam, The Netherlands*

† Electronic supplementary information (ESI) available. See DOI: https://doi.org/10.1039/d4ra05464d

LIBs are $LiCoO_2$ (LCO),[3,4] $LiMnO_2$ (LMO),[5,6] $LiFePO_4$ (LPO)[7–9] and $Li[Ni_xMn_yCo_z]O_2$ (NMC).[10] For long lifetime and large energy storage LIBs, the use of nickel-rich NMC layered cathodes can be considered as an excellent approach to reconcile the requirement of high specific discharge capacity, reasonable durability and working voltages, and affordable production cost.[11] In the case of anode materials, the most common electrode material for commercial lithium-ion rechargeable batteries is graphite.[12] The advantages of graphite electrodes are their low price, large reserves, and high conductivity. However, a disadvantage is its low maximum storage capacity (372 mA h g^{-1}) due to the very flat surface and the fact that the charge/discharge rate tends to decrease rapidly after each charge/discharge cycle because of the formation of solid–electrolyte interface (SEI).[13] Therefore, the search for new electrode materials that possess the superior properties of graphite electrodes but can overcome their inherent disadvantages (storage capacity and ionic diffusion ability) is a major challenge in the lithium-ion rechargeable battery industry.

In 2015, Zhang *et al.* theoretically proposed two-dimensional T12-carbon penta-graphene (PG) as a completely new type of hypothetical carbon material assembled from carbon atoms with pentagonal patterns.[14] These PG sheets have intrinsic indirect bandgap of 3.25 eV, predicted by computations using the Heyd–Scuseria–Ernzerhof (HSE06) exchange–correlation functional of density functional theory, and are thermally stable at temperatures up to 1000 K. In 2016, using density functional theory and molecular dynamics simulations, Xiao *et al.* theoretically showed that albeit penta-graphene sheets are mechanically less stable than graphite monolayers, their maximum storage capacity and average open circuit voltage (OCV) and electron diffusion barrier amount to 1489 mA h g^{-1}, 0.55 V and 0.17 eV, respectively, making them outstanding candidates for lithium-ion battery anodes.[15] By cutting the PG sheets along different crystallographic directions, we can obtain penta-graphene nanoribbons (PGNR).[16] These nanoribbons exhibit a high carrier mobility ranging from $\sim 10^1$ to $\sim 10^4$ cm^2 V^{-1} s^{-1} at room temperature depending on the edge-terminated atoms.[17] With hydrogen termination at the edges, the PGNR behaves as a semiconductor with a bandgap of ~2.4 eV[17] and a low energy diffusion barrier of 0.40 eV.[18] Furthermore, within this pentagonal world of materials, penta-silicene and penta-germanene have been synthesized successfully using the *in situ* molecular beam epitaxy on gold (110)[19–22] and (111)[23] surfaces, respectively. This demonstrates the potential synthesis success and application of penta-graphene materials on advanced electronic materials.

Recently, substantial progress has been made to meet the fast-charging requirement by applying external magnetic[24,25] or electric fields.[26] Recent experimental reports demonstrate that the charge rates of LIBs can significantly be improved by imposing an external magnetic field parallel to the material surface to reduce the Li-ion transmission paths and increase the diffusion coefficients.[25] For instance, by applying an external electric field on lithium hexafluorophosphate ($LiPF_6$) in ethylene carbonate, Kumar and Seminario[27] showed a strong impact of the electric field on the mobility of lithium ions by improving the drift velocities in ethylene carbonate electrolyte. Specifically, while the diffusion coefficient is increased linearly under a small applied electric field with magnitude below 2 V nm^{-1}, it turns out to increase exponentially when an electric field strength is above that threshold.[27] Besides the common use of the electric fields on the electrolytes, more interestingly, by constructing heterojunctions assembled by nanomaterials with different bandgaps, recent experimental and theoretical reports[28–31] demonstrated the ability for building built-in electric field across the material interfaces to boost the electron and/or ion mobility. For instance, by creating a built-in electric field across the p–n junction of P-Co_3O_4/TiO_2 anode, Kong *et al.* obtained a remarkable rate capability of 801 mA h g^{-1} even after 1600 cycles at 2 A g^{-1}.[28] Fast-charging anodes with high ionic conductivity can be controlled effectively under an external electrical field.

In this context, we set out to employ first-principles methods computations with density functional theory and the climbing image nudged elastic band (CI-NEB) method to investigate the Li-ion adsorption, electronic band structure modification, and ionic diffusion and conductivity for PGNR anodes in lithium-ion batteries. The CI-NEB[32] has been known as an effective method to find the minimum reaction paths and determine the corresponding energy barriers between the given initial and final configurations. During optimization, this method creates a set of images to connect the initial and final states by performing a linear interpolation between the neighboring images to find the highest energy image of the transition state structure. In this paper, we report on the greatly improved electrochemical properties of penta-graphene anodes resulting from the change in structural stability, density of states, ionic diffusion and transition energy following application of electric fields. Such an improvement points out the potential application of penta-graphene nanoribbons as anode materials for the next generation of lithium-ion rechargeable batteries.

2. Computational methods

2.1 Methods for structural optimizations

In this study, all periodic DFT optimizations are performed using the projector-augmented wave (PAW) method[33] implemented in the Vienna *ab initio* simulation package (VASP).[34,35] Upon adsorption, the interaction between the graphene-like materials and the adsorbants is mainly governed by the long-range van der Waals (vdW) interaction.[36,37] Therefore, for geometrical optimizations, we include the optB86b-vdW[38] exchange–correlation functional in the vdW-DF family to obtain the optimized configurations closely match to the experimental observations. The integration in the Brillouin zone was employed using the Monkhorst–Pack scheme[39] ($11 \times 1 \times 1$) with an energy cut-off of 500 eV. The convergence threshold for the self-consistent field calculations was set to 10^{-5} eV per cell, and the geometrical structures were fully optimized until the Hellmann–Feynman forces acting on atoms were less than 0.01 eV $Å^{-1}$. To avoid the boundary effect on the interatomic layers of PGNR, a vacuum of 20 Å is applied between two neighboring nanoribbons.

To determine the most stable of PGNR with a single Li atom, we place the Li atom 3 Å above the top layer of the PGNR at all possible adsorption sites as shown by letters A–I in Fig. 1(a). The stability of the adsorption configurations is evaluated by the formation energy as follows[40]

$$E_{\text{Form}} = \frac{E_{\text{total}} - n_{\text{C}}E_{\text{C}} - n_{\text{H}}E_{\text{H}} - n_{\text{Li}}E_{\text{Li}}}{n_{\text{C}} + n_{\text{H}} + n_{\text{Li}}},$$

in which E_{total} is the total Gibbs free energy of the adsorption systems, E_{C}, E_{H}, E_{Li} stand for the chemical potentials of C, H, Li atoms. The symbols n_{C}, n_{H}, n_{Li} are the number of C, H, Li atoms in the hosted PGNR samples.

2.2 Methods for calculating the band structures

The conventional exchange correlation functionals usually underestimate semiconductor band gap whereas hybrid functionals can bridge the gap between DFT simulations and experimental observations.[41] To study the band structures of the pristine PGNR and the PGNR upon lithium adsorption at high accuracy, we apply the Heyd–Scuseria–Ernzerhof (HSE06)[42] hybrid functional implemented in the VASP (with the *k*-point grid of 7 × 1 × 1 in the Monkhorst–Pack scheme) and in the BAND engine of the Amsterdam Modeling Suite (AMS)[43] packages. For the band structure and density of state calculations in the BAND engine, we apply the triple zeta polarization (TZP) basic sets with the core orbitals considered as frozen during the self-consistent field procedure.

For further analyses of orbital hybridization, we perform the periodic energy decomposition analyses (PEDA) using the BP86-D3 exchange–correlation potential with the same basic sets in the AMS package. Since the HSE06 functional is not yet implemented in the AMS package for decomposing the interaction energies, we use the BP86-D3 functional, which is identical to the exchange–correlation optB86b-vdW functional in VASP package.

2.3 Methods for obtaining diffusion barriers

The charge/discharge capability is an essential factor to determine whether a proposed material is suitable for developing an anode material for lithium-ion batteries. To characterize the diffusion behavior of lithium ions, we use the climbing image-nudged elastic band (NEB)[32,44] implemented in the AMS package. The initial and final states are taken systematically from the geometrical optimization procedure in VASP. For each migration path, sixteen intermediate images are used during the NEB image calculations.

3. Results and discussion

3.1 Adsorption of Li-ion on penta-graphene nanoribbons

To evaluate the effect of an external electric field on the electronic band structures and ionic diffusion properties of PGNR upon lithium adsorption, we perform DFT optimization on a PGNR with a width of nine sawtooth carbon chains to obtain the most stable pristine configuration as shown in Fig. 1(a). The C atoms are distributed in three hierarchical atomic planes with a roughness of $d \approx 0.768$ Å. The thickness of these nanoribbons (measured from the top to the bottom layers of C atoms) is $h = 1.412$ Å. There are two types of C–C bonds in the pristine PGNR: C–C single bonds with a length of ∼1504–1569 Å and C=C double bonds with a length of ∼1337–1341 Å. The sp^2 hybridized carbon atoms with three coordination numbers (denoted as C_1 atoms) are located in the middle layer, while the sp^3 carbon atoms with four coordination numbers (C_2) lie in the bottom and top layers (Fig. 1(a)–(c)). These results agree well with previous reports.[14,16,45] To further evaluate the stability of PGNR, we also calculate its phonon dispersion spectra. As shown in the phonon spectra of Fig. S1(a),† these ribbons are dynamically stable due to the absence of imaginary modes, and we also observe distinct acoustic modes close to the *Γ*-point,

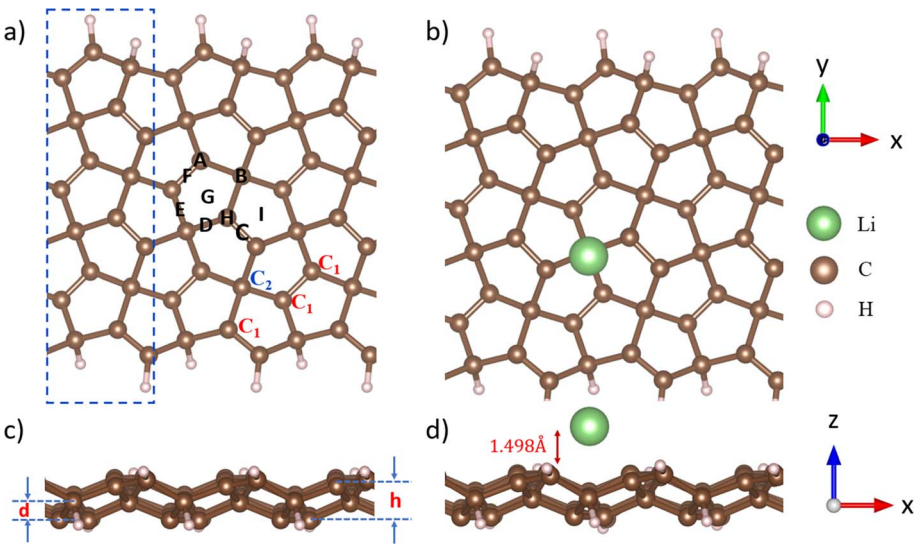

Fig. 1 Top- and side-view of the optimized geometrical structures of PGNR (a–c) and PGNR + Li (b and d). The yellow, gray and white balls illustrate Li, C and H atoms, respectively. The possible Li adsorption sites (a) are marked as on top (A, B, H), at hollow (I, G), and in the bridge (C, D, E, F) of C atoms. The dashed blue rectangle represents the supercell of PGNR.

Table 1 Formation energies E_{ads} and adsorption distances a from the Li atom to PGNR at different adsorption sites

Site	A	B	C	D	E	F	G	H	I
E_{ads} (eV)	−0.219	−0.219	−0.216	−0.220	−0.220	−0.219	−0.218	−0.218	−0.219
a (Å)	1.345	1.444	1.943	1.498	1.491	1.014	1.026	1.031	1.148

illustrating the typical out-of-plane, in-plane longitudinal, and in-plane transverse atomic motions typical for (penta-)graphene, as thoroughly discussed in ref. 14.

To investigate the adsorption of Li atoms, we evaluate the structural stability upon adsorption of a single Li atom on nine possible adsorption sites of the most stable PGNR configuration (Fig. 1(a)). Table 1 presents the formation energy E_{ads} and the corresponding adsorption distances of all possible adsorption sites. The adsorption distance is the center-to-center distance from the adsorbed Li atom to the nearest C atoms of the PGNR.

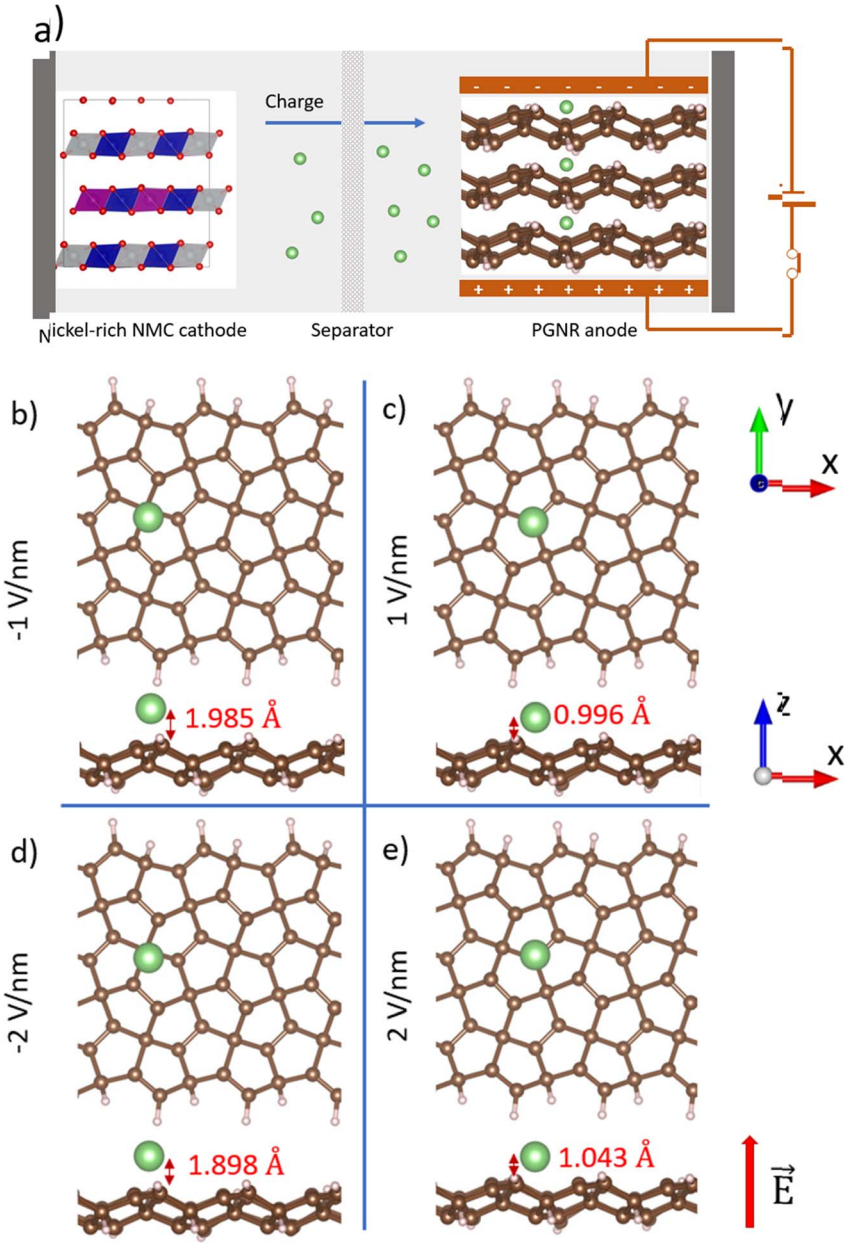

Fig. 2 (a) Sketch of a lithium-ion battery with a penta-graphene nanoribbon anode under a vertical electric field. The geometrical structures with top and side views of these adsorbed system under an electric field of −1 V nm^{-1}. (b), 1 V nm^{-1}, (c), −2 V nm^{-1}, (d) and 2 V nm^{-1} (e). The positive direction of the external electric field is sketched at the bottom right of figure (e). The shortest distances from the adsorbed lithium-ion to PGNR are also displayed in these figures.

As shown in Table 1, the lowest adsorption energy of all possible adsorption sites is −0.220 eV at the *D* and *E* sites. Furthermore, after equilibration, irrespective of the initial configurations at *D* or *E* sites, the adsorbed Li atom relaxes on top of the sp^3 hybridized C atom, illustrating that the sp^3 configuration is the most energetical stable one. The fundamental phonon dispersion characteristic remains almost unchanged for these nanoribbons upon lithium adsorption (Fig. S1b†). Thus, for the further calculations, we associate the PGNR with a Li atom on top of the sp^3 C atom as the most stable configuration.

We now apply an electric field perpendicular to the surface of the penta-graphene nanoribbons. The field is applied to all atoms in the adsorbed systems *via* the Kohn–Sham equations. This artificial field is to mimic the built-in electric field, *i.e.*, generated in between the p–n junction of a heterostructure anode as reported in ref. 28. Note that since this electric field is perpendicular to the surface of the ribbons, this force will not perform work to the moving carriers parallel to the surface of the ribbons. The strength of the applied field varies from −2 V nm^{-1} to 2 V nm^{-1} with a stepsize of 1 V nm^{-1}, where positive (negative) values indicate a field in the positive (negative) *z*-direction. This field is strong enough to disturb the electron diffusion process but is weak enough not to destroy the adsorption system. Under a positive electric field, the adsorbed Li atom is relaxed on top of the sp^2 hybridized carbon atom as indicated in Fig. 2. However, under a negative electric field, the adsorbed Li atom anchors close to the top of the sp^3 hybridized carbon atom. To evaluate the stability of these configurations, we calculate the relative energy difference which is the energy difference between the systems with the electric field and the one without it. As shown in Table 2, the adsorption systems are slightly more stable with applied electric field than without, as indicated by the negative values of the relative energy difference. Apart from that, the lattice constant in the *x*-direction and the buckling distance (being the furthest distance between two carbon atoms in the *z* direction of the PGNR) of the systems show minor changes with the largest buckling of 9.75%.

Although there is a presence of a negative dispersion band when these nanoribbons are placed under a positive electric field (Fig. S1c and d†), in general, these ribbons are mechanically stable under these small electric fields. The most interesting observation is that the Li atom is adsorbed more closely to the PGNR when a positive electric field is applied. As shown in Fig. 2, the adsorption distance from the Li atom to the PGNR reduces by about 30% when the field is applied in the *z*-direction, while for fields in the opposite direction, this quantity extends by about 30% with respect to the field-less case. This implies significant changes of the ionic diffusion and conductivity of the adsorbed systems under an external electric field, as discussed in the next section.

3.2 Effects of an electric field on the electronic band structures of Li-ion penta-graphene nanoribbons

To increase the accuracy as well as the reliability of the calculated electronic properties, we further calculate the band structure and partial density of states of these adsorbed systems using the HSE06 hybrid functionals.[46] As shown in Fig. 3, S2 and S3 (ESI file†), the PGNR exhibits semiconductor properties with an indirect band gap of 3.415 eV or 3.433 eV, as calculated by the AMS and VASP packages, respectively. These results are in quantitative agreement with the previous report of 3.25 eV[14] for a two-dimensional penta-graphene system. The electronic energy states are mainly dominated by the 2-p_z orbitals of carbon atoms (Fig. S3, ESI file†), illustrating the high possibility for orbital hybridation in the *z* direction. The localized π electrons of sp^2 carbon atoms are also well visualized by the shapes of frontier orbitals (both the highest occupied molecular orbital (HOMO) and the lowest unoccupied molecular orbital (LUMO) states) on the top-left of Table 3, which is typical for penta-graphene nanoribbons.[47]

Upon lithium adsorption, the semiconductor PGNR becomes metal as indicated in Fig. 4, in line with previous reports.[14,48] This semiconductor-to-metal transition demonstrates that PGNR is a good anode material for lithium-ion batteries due to creation of free charges from the interaction between the adsorbed Li atoms and C atoms of the PGNR. The energy states around the Fermi level are driven by the π electrons of carbon atoms as displayed in Fig. S4 (ESI file†), demonstrating a charge transfer from the adsorbed Li atom to the PGNR as pointed out in ref. 48 and a high possibility of hybridization between p-orbital of the C and s-orbital of the Li atom. The significant contribution of the Li-atom's s-orbital to

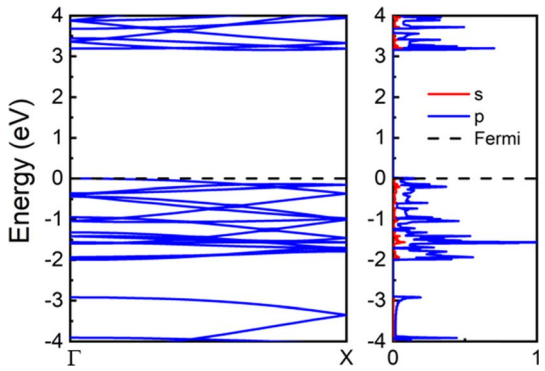

Fig. 3 Band structure and partial density of states of penta-graphene nanoribbons calculated in the AMS package. The Fermi level indicated by the dashed lines is set to zero.

Table 2 The structural modification of the PGNR under an applied electric field

Electric field strength (V nm^{-1})	−2	−1	0	1	2
Relative energy difference (eV)	−0.018	−0.162	0	−0.084	−0.169
Lattice constant in *x*-direction (Å)	10.854	10.854	10.857	10.854	10.855
Buckling distance (Å)	0.642	0.743	0.677	0.712	0.667

Table 3 Shapes of frontier orbitals of PGNR and PGNR upon lithium adsorption in the absence and under an external electric field in top (upper images) and side (lower images) views. These shapes are calculated in the AMS package. Iso-value for the orbital rendering is 0.02 eV Å^{-2}. The electron depletion is in blue whereas the electron accumulation is in reddish brown

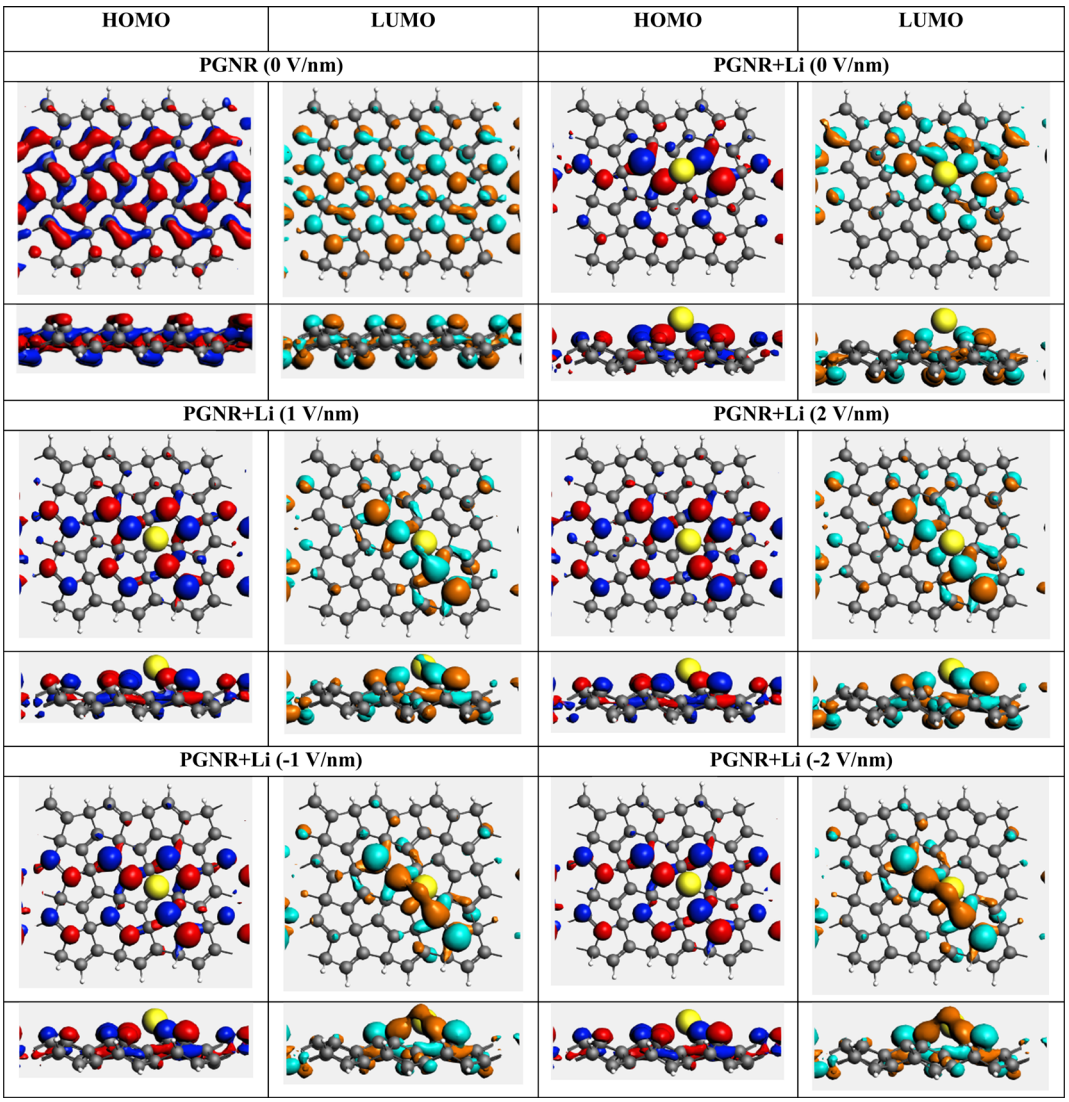

the density of states close to the Fermi level cause an increase in the conductivity of PGNR upon lithium adsorption and lead to the semiconductor-to-metal transition. Additionally, the interaction with the Li atom can enhance the flexibility of p-orbital electrons of the C atoms, leading to a strong shift of the highest occupied molecular orbital (HOMO) towards the bottom of the conduction band (*cf.* Fig. 4 and S4, ESI file†). The electrons transferred from the Li atom, and the flexible p-orbital electrons of the C atoms occupying the HOMO may play an important role in increasing the electronic conductivity of the PGNR + Li systems.

A significant band modification of the PGNR + Li under an external electric field is clearly visible in Fig. 4. Under a 2 V nm^{-1} electric field, we observe a considerable down-shift of the band dispersion curves in the conduction band towards the Fermi level while this trend is less pronounced in the case of a −2 V nm^{-1} electric field. Similar behavior is also observed in

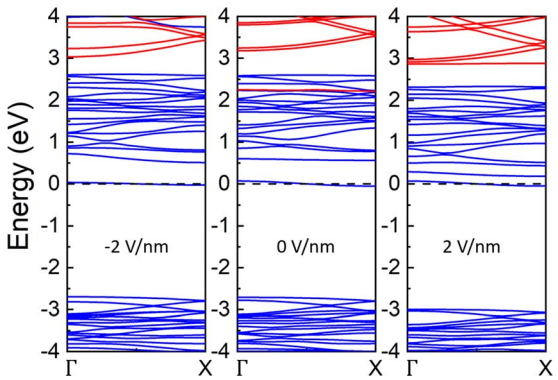

Fig. 4 Band structure of penta-graphene nanoribbons upon lithium adsorption calculated in the AMS package. Red and blue lines represent for the s- and p-orbitals. The Fermi level indicated by the dashed lines is set to zero.

Fig. S4 (ESI file†) obtained from the VASP package. Furthermore, under a positive applied electric field, a new state appears in the conduction band just above the Fermi level. This state is occupied by s-orbitals of the adsorbed Li atoms, increasing its pDOS compared to nearby states (Fig. S4†) further increasing the conductivity of PGNR + Li under positive electric fields. We would stress that these modifications of the band structure and pDOS are different from those under negative electric field; hence, the applied field direction exerts a strong impact on the electronic characteristics of the PGNR + Li systems.

The electrons of frontier orbitals play an important role, in part governing the electronic properties of the material. To get further insights into the change in electronic properties of PGNR caused from the Li adsorption, and the effect of the external electric field, we probe the modification of the local electron distribution of HOMO and LUMO states of the material. Table 3 displays the shapes of frontier orbitals of pristine PGNR, PGNR + Li without and with an external electric field. For pristine PGNR (without applied external electric field), electrons of the HOMO and LUMO mainly localize around sp^2 C atoms and distribute over the areas inside the PGNR like that observed for PG.[14] The density of electrons of these two states around C atoms at the edge of the nanoribbon is inconsiderable, possibly, due to effect of the H passivation. Upon lithium adsorption, the distribution of electrons of the HOMO and LUMO exhibits a higher localization. They are mainly concentrated on the top of C atoms near the adsorbed Li atom with relative high density and could act as free electrons, leading to an increase of the electronic conductivity of PGNR upon adsorption. Such a redistribution of electrons of the frontier orbitals due to the Li adsorption also results the transition from the conductor-to-metal behavior of PGNR. As shown in Table 3, under an electric field, the LUMO states are more locally placed around the adsorbed Li atoms. Such a change of the LUMO orbital shapes implies a strong increase of the conductivity of PGNR + Li under the external electric field. Interestingly, Table 3 also shows that under a negative electric field, the electron depletion areas of frontier orbitals are replaced by the accumulation areas, whereas this phenomenon is not observed when applying a positive field, demonstrating the dependence of electronic properties of the PGNR + Li systems on the direction of the applied fields.

To further understand the influence of external electric fields on the electronic properties of the adsorbed systems, we perform periodic energy decomposition analyses (PEDA) to calculate the intrinsic bond energy ΔE_{int} consisting of the electrostatic energy ΔE_{eslast}, the Pauli repulsion energy ΔE_{Pauli}, and the orbital relaxation energy between the adsorbed lithium atom (the first fragment) and all other carbon atoms (the second fragment including 54 carbon and 12 hydrogen atoms) according to eqn (1):

$$\Delta E_{int} = \Delta E_{eslast} + \Delta E_{Pauli} + \Delta E_{orb}, \quad (1)$$

The computed intrinsic bond and partial energies are given in Table 4. Note that the relatively high energy values in Table 4 are summed over each fragment. These indicate that a weak

Table 4 Periodic energy decomposition analyses (PEDA) of PGNR upon lithium adsorption calculated in the AMS package. All units are in kJ mol^{-1}

PEDA types	$E = -2$ V nm^{-1}	$E = 0$ V nm^{-1}	$E = 2$ V nm^{-1}
ΔE_{int}	−41.9	−64.9	−62.2
ΔE_{eslast}	−318.5	−418.3	−670.2
ΔE_{orb}	−183.0	−249.4	−367.6

external electric field can modify the intrinsic bond energies and their parts, by modifying the interaction between PGNR and Li atoms. Looking in more detail, the electrostatic energy emerges as the most dominant factor in the absence or presence of external electric fields, illustrating that the interaction between PGNR and Li is mainly driven by electrostatic effects, and the adsorbed Li atoms yield considerable electronic contributions to the PGNR. Looking at the orbital relaxation energies, which cover the orbital hybridization effect in the adsorption system, with respect to the zero electric field, the magnitudes of this quantity tend to decrease under a negative electric field and increase significantly under the positive field, again indicating the sensitivity of these adsorbed systems under an external electric field. The increase in electrostatic energy under positive electric field results from a charge redistribution of the frontier orbital and the nearby states as shown in Table 3 and Fig. S4 (ESI file†). Hence, the enhanced charge distribution of the adsorbent and adsorbate originates from charge transfer due to the reduced distance between the Li and PGNR as pointed out above. As a result, the diffusion coefficient of Li ions on PGNR under positive electric field is significantly higher than that without and under a negative field. On the other hand, the smaller orbital relaxation energy under negative electric fields, implies a weakening of the orbital hybridization between the adsorbed Li and the PGNR. Therefore, positive electric fields enhance the flexibility of the p-orbital electrons of C atoms; and these results anticipate an increase of the conductivity as well as the diffusion coefficient of Li ions on the adsorbed systems.

3.3 Effects of an electric field on the diffusion process of Li-ion penta-graphene nanoribbons

The diffusion energy profiles, and the energy barriers of lithium-ion migration are an essential factor for evaluating the performance of lithium-ion anodes. A low energy barrier indicates that the lithium-ions can easily migrate along preferable diffusion paths. In this section, we investigate the effect of an external electric field on the lithium-ion diffusion characteristics of penta-graphene nanoribbons. As discussed above, under a zero and negative electric fields, the adsorbed lithium atoms are energetically stable on top of the sp^3 hybridized carbon atoms while under the positive fields, the equivalent stabilized positions are on top of the sp^2 carbon atoms. The diffusion paths are chosen as the shortest paths between the two most energetically favorable configurations as illustrated by red arrows in Fig. 5.

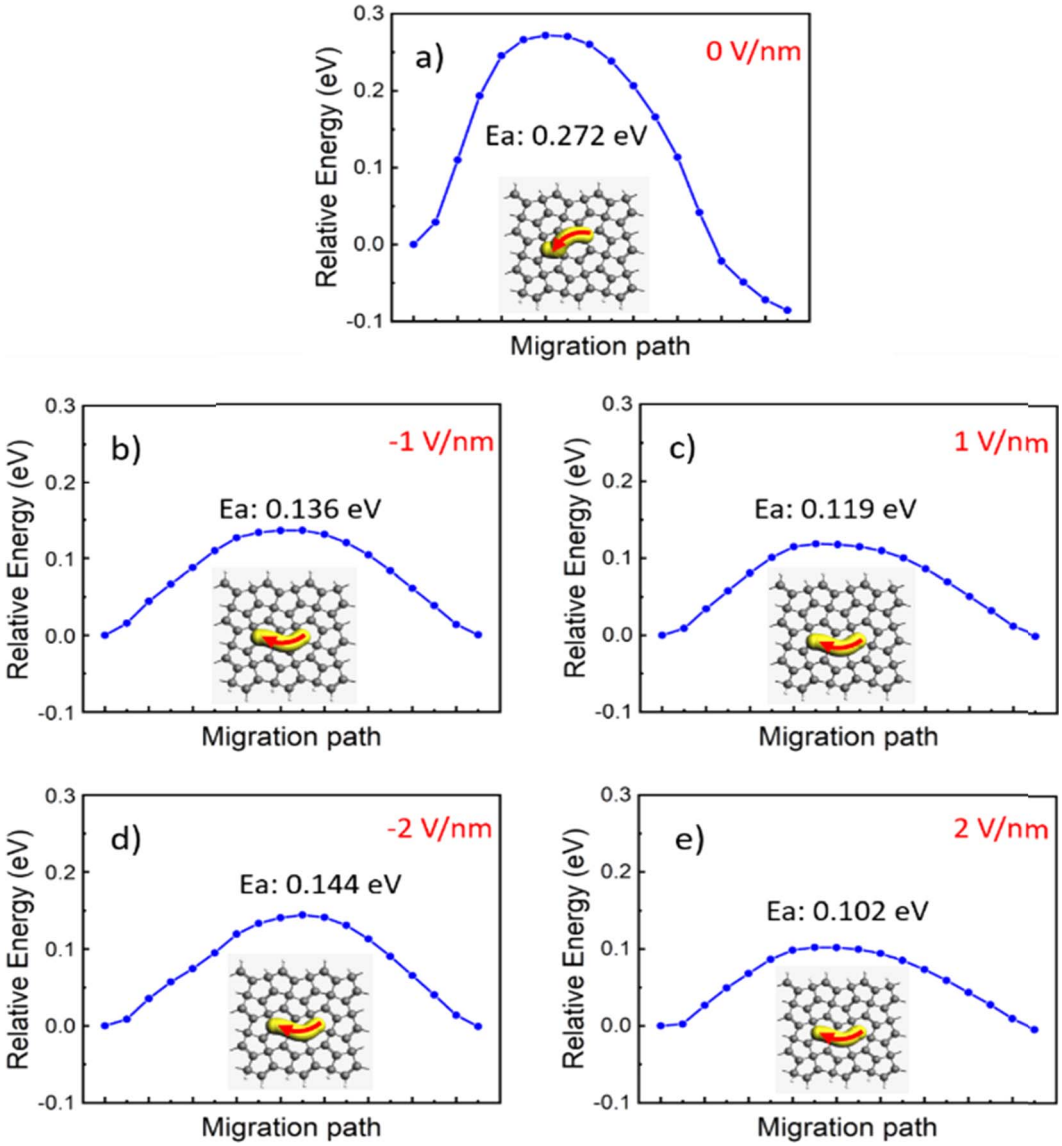

Fig. 5 Diffusion barriers of lithium-atoms on penta-graphene nanoribbons under an external electric field.

In the absence of an electric field, the diffusion barrier calculated by the CI-NEB method along the diffusion path highlighted in Fig. 5a is 0.272 eV, which is in quantitative agreement with that of two-dimensional penta-graphene ($\leq$0.33 eV),[15] comparable to the case of penta-hexagonal graphene (in between 0.21 eV and 0.32 eV)[49] and significantly lower than those of commercial graphite anodes (0.4–0.6 eV)[49] and $LiFePO_4$ (1.02 eV) electrodes.[50]

In the presence of an external electric field, this diffusion barrier significantly reduces to the lowest value of ~0.1 eV at 2 V nm^{-1} electric field as shown in Table 5 and Fig. 5. Such low diffusion barrier, which is comparable with that of Ti_3C_2 (ref.

Table 5 Diffusion barrier and diffusion coefficient of lithium-ions on penta-graphene nanoribbons under an external electric field

Electric field strength (V m^{-1})	−2	−1	0	1	2
Diffusion barrier (eV)	0.144	0.136	0.272	0.119	0.102
Diffusion coefficient (cm^2 s^{-1})	4.5×10^{-4}	6.2×10^{-4}	3.2×10^{-6}	1.2×10^{-3}	2.3×10^{-3}
The lithium diffusion coefficient ratio between penta-graphene nanoribbons and graphitic carbon[55]	102.78	139.99	0.73	269.98	520.71
Conductivity (S cm^{-1})	1.74×10^{-2}	2.40×10^{-2}	1.24×10^{-4}	4.64×10^{-2}	8.89×10^{-2}

49) and the recent proposed MoS_2/penta-graphene heterostructures,[51] strongly demonstrates the remarkable fast ion diffusion of penta-graphene nanoribbons under an applied electric field.

The diffusion coefficient of lithium-ions can be calculated *via* the relation (2)

$$D = a^2 \nu e^{-\frac{E_{act}}{k_B T}} \quad (2)$$

where a is the diffusion length of ions, $\nu \sim 1013$ Hz, k_B is Boltzmann's constant, T is the room temperature ($T = 300$ K),[50] and E_{act} stands for the diffusion barrier. Furthermore, we also estimate the ionic conductivity using the Nernst–Einstein relation[52–54] (eqn (3)):

$$\sigma(T) = H_V N q^2 D(T)/k_B T \quad (3)$$

where q is the charge of the mobile ion, N the charge density of the mobile ion, k_B the Boltzmann constant, and H_V represents the Haven's ratio used to consider the effect on the mobility of the charge carriers under an external electric field, which is considered equal to 1.

As shown in Table 5 and in the absence of an electric field, the lithium-ion diffusion coefficient and conductivity of penta-graphene nanoribbons are 3.2 × 10−6 $cm^2\ s^{-1}$ and 1.24 × 10^{-4} S cm^{-1}, respectively, while under an external electric field, these quantities increase significantly. Specifically, under a positive electric field of 1 V nm^{-1} and 2 V nm^{-1}, it reaches to 1.2 × 10^{-3} $cm^2\ s^{-1}$ and 2.3 × 10−3 $cm^2\ s^{-1}$, which is approximately about ∼375 and ∼719 times faster than that of the case of zero electric field, respectively. Under negative electric fields, though we also observe an increase of diffusion coefficients, these quantities are relatively smaller than in the case of positive electric fields. These observations are in line with the additional electronic states formed in the conduction bands close to the Fermi level (Fig. 4).

A similar behavior is also observed in the case of ionic conductivity. To demonstrate the outperformance of PGNR as a promising material for lithium-ion anodes, we compare our calculated diffusion coefficients with those of carbon graphite layers, a common electrode material of commercial batteries.[55] Table 5 illustrates that the diffusion coefficient of PGNR under a zero electric field is slightly lower that of graphitic carbon layers but reaches ∼521 times higher under a 2 V nm^{-1} electric field. Therefore, the external electric field can be used as a novel switch to remarkably improve the charge/discharge rate of penta-graphene lithium-ion anodes.

Besides the diffusion barrier, diffusion coefficient and conductivity, another essential factor which greatly contributes to the charge/discharge rates of lithium-ion anodes is the electronic conductivity, which can be inferred by carrier effective mass.[56]

The effective masses of electrons (m_e^*) and holes (m_h^*) are calculated from eqn (4)

$$m^* = \hbar^2 \left(\frac{d^2 E(k)}{dk^2} \right)^{-1} \quad (4)$$

Table 6 Effective masses of electrons (m_e^*/m_0) and holes (m_h^*/m_0) of penta-graphene nanoribbons upon adsorption of lithium-ions under an external electric field

Electric field (V nm^{-1})	−2	−1	0	1	2
m_h^*/m_0	0.865	0.863	0.842	0.864	0.865
m_e^*/m_0	0.217	0.145	1.442	0.036	0.033
m_h^*/m_e^*	3.986	5.952	0.584	24.000	26.212

where $\hbar$ is the Planck's constant, k and $E(k)$ are respectively the wave vector and the energy dispersion relation corresponding to the conduction-band minima and valence-band maxima[50] of Fig. 3 and 4. The effective masses of holes and electrons of pristine PGNR are $0.852m_0$ and $0.519m_0$ (where m_0 is the mass of an electron), respectively, that are larger than the effective masses of holes and electrons in two-dimensional penta-graphene ($0.50m_0$ and $0.24m_0$, respectively[57]). These results indicate that holes and electrons of pristine penta-graphene nanoribbons are less mobile than those of penta-graphene monolayers. Upon lithium adsorption, the effective mass of electrons becomes $1.442m_0$ which is ∼2.8 times larger than that of pristine PGNR, and the m_h^*/m_e^* is 0.584, meaning that these electrons are even less mobile than in the case of pristine systems. However, under an external electric field, these m_h^*/m_e^* effective mass ratios increase dramatically.

While under the negative electric fields, these ratios increase a few times, in the opposite electric field directions, we observe remarkable increases up to ∼26 times higher (see Table 6). Obviously, this sudden increase of the m_h^*/m_e^* ratios highlights the role of an external electric field as a novel switch to improve the conductivity of penta-graphene lithium-ion anodes.

4. Concluding remarks

We presented in detail the remarkable effects of an external electric field which enhances the ionic conductivity and the lithium-ion diffusion coefficients of penta-graphene nanoribbons upon adsorption of lithium atoms. The adsorbed systems are as thermodynamically stable as the pristine systems. Following adsorption of lithium atoms, the semiconductor penta-graphene nanoribbons become metal, originating from the orbital hybridization between the sp^3 carbon atoms and the lithium atoms. The PGNR anode materials exhibit fast diffusion coefficient of ∼521 times higher than that of carbon graphite layer. The external electric field can be used as a novel switch to improve the efficiency of lithium-ion batteries with penta-graphene nanoribbon anodes. Furthermore, these electric fields support directional orientations of lithium-ion conductivity and diffusion barriers, and penta-graphene nanoribbons promise an excellent anode material for lithium-ion batteries with ultrafast charge/discharge rates. Further experimental investigations on pentagonal class of materials are highly desirable to shed light on these promising materials for applications in lithium-ion batteries.

Data availability

The data supporting this article have been included as part of the ESI.†

Conflicts of interest

There are no conflicts of interest to declare.

Acknowledgements

This research is funded by the Ministry of Education and Training, Vietnam (under Grant number B2024-TCT-16) and VinUniversity Seed Funding Program 23-24. The authors acknowledge the Information and Network Management Centre at Can Tho University for providing high-performance computing resources.

References

1 P. I. Penafort, *Lithium-ion batteries – statistics & facts*, Statista, 2024, https://www.statista.com/topics/2049/lithium-ion-battery-industry/#topicOverview.
2 W. Zuo, A. Innocenti, M. Zarrabeitia, D. Bresser, Y. Yang and S. Passerini, Layered oxide cathodes for sodium-ion batteries: storage mechanism, electrochemistry, and techno-economics, *Acc. Chem. Res.*, 2023, **56**(3), 284–296, DOI: 10.1021/acs.accounts.2c00690.
3 K. Ozawa, Lithium-ion rechargeable batteries with $LiCoO_2$ and carbon electrodes: the $LiCoO_2$/C system, *Solid State Ionics*, 1994, **69**(3), 212–221, DOI: 10.1016/0167-2738(94)90411-1.
4 Y. Lyu, et al., An overview on the advances of $LiCoO_2$ cathodes for lithium-ion batteries, *Adv. Energy Mater.*, 2021, **11**(2), 2000982, DOI: 10.1002/aenm.202000982.
5 X. Zhu, et al., $LiMnO_2$ cathode stabilized by interfacial orbital ordering for sustainable lithium-ion batteries, *Nat. Sustainability*, 2021, **4**(5), 392–401, DOI: 10.1038/s41893-020-00660-9.
6 H. Zhao, et al., Orthorhombic $LiMnO_2$ nanorods as cathode materials for lithium-ion batteries: synthesis and electrochemical properties, *Ceram. Int.*, 2016, **42**(7), 9319–9322, DOI: 10.1016/j.ceramint.2016.01.207.
7 Y. Zhang, et al., Advances in new cathode material $LiFePO_4$ for lithium-ion batteries, *Synth. Met.*, 2012, **162**(13), 1315–1326, DOI: 10.1016/j.synthmet.2012.04.025.
8 S.-P. Chen, D. Lv, J. Chen, Y.-H. Zhang and F.-N. Shi, Review on defects and modification methods of $LiFePO_4$ cathode material for lithium-ion batteries, *Energy Fuels*, 2022, **36**(3), 1232–1251, DOI: 10.1021/acs.energyfuels.1c03757.
9 J. Gai, J. Yang, W. Yang, Q. Li, X. Wu and H. Li, Lithium ion batteries operated at −100 °C, *Chin. Phys. Lett.*, 2023, **40**(8), 086101, DOI: 10.1088/0256-307X/40/8/086101.
10 R. Jung, M. Metzger, F. Maglia, C. Stinner and H. A. Gasteiger, Chemical *versus* electrochemical electrolyte oxidation on NMC111, NMC622, NMC811, LNMO, and conductive carbon, *J. Phys. Chem. Lett.*, 2017, **8**(19), 4820–4825, DOI: 10.1021/acs.jpclett.7b01927.
11 R. Tatara, et al., Enhanced cycling performance of Ni-rich positive electrodes (NMC) in li-ion batteries by reducing electrolyte free-solvent activity, *ACS Appl. Mater. Interfaces*, 2019, **11**(38), 34973–34988, DOI: 10.1021/acsami.9b11942.
12 H. Zhang, Y. Yang, D. Ren, L. Wang and X. He, Graphite as anode materials: fundamental mechanism, recent progress and advances, *Energy Storage Mater*, 2021, **36**, 147–170, DOI: 10.1016/j.ensm.2020.12.027.
13 R. Fang, K. Chen, L. Yin, Z. Sun, F. Li and H. M. Cheng, The regulating role of carbon nanotubes and graphene in lithium-ion and lithium–sulfur batteries, *Adv. Mater.*, 2019, **31**(9), 1800863, DOI: 10.1002/ADMA.201800863.
14 S. Zhang, J. Zhou, Q. Wang, X. Chen, Y. Kawazoe and P. Jena, Penta-graphene: a new carbon allotrope, *Proc. Natl. Acad. Sci. U. S. A.*, 2015, **112**(8), 2372–2377, DOI: 10.1073/PNAS.1416591112.
15 B. Xiao, Y. chun Li, X. fang Yu and J. bo Cheng, Penta-graphene: a promising anode material as the Li/Na-ion battery with both extremely high theoretical capacity and fast charge/discharge rate, *ACS Appl. Mater. Interfaces*, 2016, **8**(51), 35342–35352, DOI: 10.1021/ACSAMI.6B12727.
16 T. Y. Mi, D. M. Triet and N. T. Tien, Adsorption of gas molecules on penta-graphene nanoribbon and its implication for nanoscale gas sensor, *Phys. Open*, 2020, **2**, 100014, DOI: 10.1016/j.physo.2020.100014.
17 Y. H. Li, P. F. Yuan, Z. Q. Fan and Z. H. Zhang, Electronic properties and carrier mobility for penta-graphene nanoribbons with nonmetallic-atom – terminations, *Org. Electron.*, 2018, **59**, 306–313, DOI: 10.1016/j.orgel.2018.05.039.
18 U. Palanivel, H.-K. Kim and Y.-C. Kim, Adsorption and migration of a single lithium on tetra-penta-hepta-graphene nanoribbon: a density functional theory approach, *Phys. Status Solidi B*, 2022, **259**(3), 2100369, DOI: 10.1002/pssb.202100369.
19 M. A. Nazir, A. Hassan, Y. Shen and Q. Wang, Research progress on penta-graphene and its related materials: properties and applications, *Nano Today*, 2022, **44**, 101501, DOI: 10.1016/j.nantod.2022.101501.
20 S. Sheng, et al., The pentagonal nature of self-assembled silicon chains and magic clusters on Ag(110), *Nano Lett.*, 2018, **18**(5), 2937–2942, DOI: 10.1021/acs.nanolett.8b00289.
21 G. Prévot, C. Hogan, T. Leoni, R. Bernard, E. Moyen and L. Masson, Si nanoribbons on Ag(110) studied by grazing-incidence X-ray diffraction, scanning tunneling microscopy, and density-functional theory: evidence of a pentamer chain structure, *Phys. Rev. Lett.*, 2016, **117**(27), 276102, DOI: 10.1103/PhysRevLett.117.276102.
22 J. I. Cerdá, J. Sławińska, G. Le Lay, A. C. Marele, J. M. Gómez-Rodríguez and M. E. Dávila, Unveiling the pentagonal nature of perfectly aligned single-and double-strand Si nanoribbons on Ag(110), *Nat. Commun.*, 2016, **7**(1), 13076, DOI: 10.1038/ncomms13076.
23 J. Zhao and H. Zeng, Chemical functionalization of pentagermanene leads to stabilization and tunable

electronic properties by external tensile strain, *ACS Omega*, 2017, **2**(1), 171–180, DOI: 10.1021/acsomega.6b00439.

24 G. Ruan, J. Hua, X. Hu and C. Yu, Study on the influence of magnetic field on the performance of lithium-ion batteries, *Energy Rep.*, 2022, **8**, 1294–1304, DOI: 10.1016/j.egyr.2022.02.095.

25 L. Zhang, M. Zeng, D. Wu and X. Yan, Magnetic field regulating the graphite electrode for excellent lithium-ion batteries performance, *ACS Sustainable Chem. Eng.*, 2019, **7**(6), 6152–6160, DOI: 10.1021/acssuschemeng.8b06358.

26 W. Shi, Z. Wang, Z. Li and Y. Q. Fu, Electric field enhanced adsorption and diffusion of adatoms in MoS2 monolayer, *Mater. Chem. Phys.*, 2016, **183**, 392–397, DOI: 10.1016/j.matchemphys.2016.08.043.

27 N. Kumar and J. M. Seminario, Lithium-ion model behavior in an ethylene carbonate electrolyte using molecular dynamics, *J. Phys. Chem. C*, 2016, **120**(30), 16322–16332, DOI: 10.1021/ACS.JPCC.6B03709.

28 H. Kong, C. Yan, C. Lv, J. Pei and G. Chen, Electric field effect in a Co_3O_4/TiO_2 p–n junction for superior lithium-ion storage, *Mater. Chem. Front.*, 2019, **3**(5), 909–915, DOI: 10.1039/C9QM00007K.

29 Y. Zhang, et al., Phase-junction engineering triggered built-in electric field for fast-charging batteries operated at -30 C, *Matter*, 2023, **6**(6), 1928–1944, DOI: 10.1016/j.matt.2023.03.026.

30 S. Subash, K. Lakshmanan, K. Vediappan and K. K. Bharathi, High Li-ion diffusion coefficient in $LiMn_{1.5}Ni_{0.5}O_4$ thin films for all-solid Li-ion battery applications, *Appl. Phys. Lett.*, 2024, **124**(2), 023903, DOI: 10.1063/5.0178190.

31 K. Chen, et al., A new generation of high performance anode materials with semiconductor heterojunction structure of SnSe/SnO_2@Gr in lithium-ion batteries, *Chem. Eng. J.*, 2018, **347**, 552–562, DOI: 10.1016/j.cej.2018.04.125.

32 G. Henkelman, B. P. Uberuaga and H. Jónsson, A climbing image nudged elastic band method for finding saddle points and minimum energy paths, *J. Chem. Phys.*, 2000, **113**(22), 9901–9904, DOI: 10.1063/1.1329672.

33 G. Kresse and D. Joubert, From ultrasoft pseudopotentials to the projector augmented-wave method, *Phys. Rev. B: Condens. Matter Mater. Phys.*, 1999, **59**(3), 1758–1775, DOI: 10.1103/PhysRevB.59.1758.

34 G. Kresse and J. Hafner, Ab initio molecular-dynamics simulation of the liquid-metalamorphous- semiconductor transition in germanium, *Phys. Rev. B: Condens. Matter Mater. Phys.*, 1994, **49**(20), 14251–14269, DOI: 10.1103/PhysRevB.49.14251.

35 G. Kresse and J. Furthmüller, Efficiency of *ab initio* total energy calculations for metals and semiconductors using a plane-wave basis set, *Comput. Mater. Sci.*, 1996, **6**(1), 15–50, DOI: 10.1016/0927-0256(96)00008-0.

36 F. Karlický, et al., Adsorption of organic molecules to van der Waals materials: comparison of fluorographene and fluorographite with graphene and graphite, *J. Chem. Theory Comput.*, 2017, **13**(3), 1328–1340, DOI: 10.1021/acs.jctc.6b01130.

37 M.-S. Zheng, S. Zhou, X. Wang and L. Gao, Understanding epitaxy of graphene: from experimental observation to density functional theory and machine learning, *J. Appl. Phys.*, 2023, **134**(9), 090901, DOI: 10.1063/5.0163580.

38 S. Grimme, J. Antony, S. Ehrlich and H. Krieg, A consistent and accurate *ab initio* parametrization of density functional dispersion correction (DFT-D) for the 94 elements H-Pu, *J. Chem. Phys.*, 2010, **132**(15), 154104, DOI: 10.1063/1.3382344.

39 H. J. Monkhorst and J. D. Pack, Special points for Brillouin-zone integrations, *Phys. Rev. B: Condens. Matter Mater. Phys.*, 1976, **13**(12), 5188–5192, DOI: 10.1103/PhysRevB.13.5188.

40 E. Perim, R. Paupitz, P. A. S. Autreto and D. S. Galvao, Inorganic graphenylene: a porous two-dimensional material with tunable band gap, *J. Phys. Chem. C*, 2014, **118**(41), 23670–23674, DOI: 10.1021/jp502119y.

41 P. J. Hasnip, K. Refson, M. I. J. Probert, J. R. Yates, S. J. Clark and C. J. Pickard, Density functional theory in the solid state, *Philos. Trans. R. Soc., A*, 2014, **372**(2011), 20130270, DOI: 10.1098/rsta.2013.0270.

42 K. Lee, É. D. Murray, L. Kong, B. I. Lundqvist and D. C. Langreth, Higher-accuracy van der Waals density functional, *Phys. Rev. B: Condens. Matter Mater. Phys.*, 2010, **82**(8), 81101, DOI: 10.1103/PhysRevB.82.081101.

43 C. J. O. Verzijl and J. M. Thijssen, DFT-based molecular transport implementation in ADF/BAND, *J. Phys. Chem. C*, 2012, **116**(46), 24393–24412, DOI: 10.1021/jp3044225.

44 G. Henkelman and H. Jónsson, Improved tangent estimate in the nudged elastic band method for finding minimum energy paths and saddle points, *J. Chem. Phys.*, 2000, **113**(22), 9978–9985, DOI: 10.1063/1.1323224.

45 B. Rajbanshi, S. Sarkar, B. Mandal and P. Sarkar, Energetic and electronic structure of penta-graphene nanoribbons, *Carbon N. Y.*, 2016, **100**, 118–125, DOI: 10.1016/J.CARBON.2016.01.014.

46 A. V Krukau, O. A. Vydrov, A. F. Izmaylov and G. E. Scuseria, Influence of the exchange screening parameter on the performance of screened hybrid functionals, *J. Chem. Phys.*, 2006, **125**(22), 224106, DOI: 10.1063/1.2404663.

47 B. Rajbanshi, S. Sarkar, B. Mandal and P. Sarkar, Energetic and electronic structure of penta-graphene nanoribbons, *Carbon N. Y.*, 2016, **100**, 118–125, DOI: 10.1016/j.carbon.2016.01.014.

48 S. Li, Y. Shen, D. Ni and Q. Wang, A new 3D metallic carbon allotrope composed of penta-graphene nanoribbons as a high-performance anode material for sodium-ion batteries, *J. Mater. Chem. A*, 2021, **9**(40), 23214–23222, DOI: 10.1039/D1TA07000B.

49 L. Lu, R. Gallenstein, X. Liu, Y. Lin, S. Lin and Z. Chen, Holey penta-hexagonal graphene: a promising anode material for Li-ion batteries, *Phys. Chem. Chem. Phys.*, 2024, **26**(9), 7335–7342, DOI: 10.1039/D3CP06146A.

50 Z. Cui, et al., Enhanced electrochemical performance and storage mechanism of $LiFePO_4$ doped by Co, Mn and S elements for lithium-ion batteries, *Electrochim. Acta*, 2021, **388**, 138592, DOI: 10.1016/J.ELECTACTA.2021.138592.

51 T. Wang, et al., First-principles study of penta-graphene/MoS_2 vdW heterostructure as anode material for lithium-ion batteries, *Diamond Relat. Mater.*, 2023, **136**, 109928, DOI: **10.1016/j.diamond.2023.109928**.

52 J. A. Dawson, T. Famprikis and K. E. Johnston, Anti-perovskites for solid-state batteries: recent developments, current challenges and future prospects, *J. Mater. Chem.*, 2021, **9**(35), 18746–18772, DOI: **10.1039/D1TA03680G**.

53 T. Famprikis, P. Canepa, J. A. Dawson, M. S. Islam and C. Masquelier, Fundamentals of inorganic solid-state electrolytes for batteries, *Nat. Mater.*, 2019, **18**(12), 1278–1291, DOI: **10.1038/s41563-019-0431-3**.

54 Y. A. Zulueta and M. T. Nguyen, Enhanced Li-ion transport in divalent metal-doped Li_2SnO_3, *Dalton Trans.*, 2021, **50**(8), 3020–3026, DOI: **10.1039/D0DT03860A**.

55 K. Persson, et al., Lithium diffusion in graphitic carbon, *J. Phys. Chem. Lett.*, 2010, **1**(8), 1176–1180, DOI: **10.1021/jz100188d**.

56 Z. El Kacemi, Z. Mansouri, A. Benyoussef, A. El Kenz, M. Balli and O. Mounkachi, First principle calculations on pristine and Mn-doped iron fluorophosphates as sodium-ion battery cathode materials, *Comput. Mater. Sci.*, 2022, **206**, 111292, DOI: **10.1016/j.commatsci.2022.111292**.

57 J. Deb, N. Seriani and U. Sarkar, Ultrahigh carrier mobility of penta-graphene: a first-principle study, *Phys. E*, 2021, **127**, 114507, DOI: **10.1016/j.physe.2020.114507**.